Ceramics International 48 (2022) 173–178

Contents lists available at ScienceDirect

Ceramics International

journal homepage: www.elsevier.com/locate/ceramint

Chromium in lead metasilicate glass: Solubility, valence, and local environment via multiple spectroscopy

David V. Sampaio [a,b,*], Rafaella B. Pena [a], Benjamin J.A. Moulton [a], Marcos V. Rezende [c], Deyvid do C. Silva [c], Ronaldo S. Silva [c], Thiago R. da Cunha [a], Valmor R. Mastelaro [d], Edgar D. Zanotto [e], Paulo S. Pizani [a]

[a] Universidade Federal de São Carlos, Departamento de Física, Caixa Postal 676, 13565-905, São Carlos, SP, Brazil
[b] Universidade Federal de Alagoas, Instituto de Física, 57072-900, Maceió, AL, Brazil
[c] Grupo de Nanomateriais Funcionais, Departamento de Física, Universidade Federal de Sergipe, 49100-000, São Cristóvão, SE, Brazil
[d] Instituto de Física de São Carlos, Universidade de São Paulo, 565-905, São Carlos, SP, Brazil
[e] Universidade Federal de São Carlos, Departamento de Engenharia de Materisais, Caixa Postal 676, 13565-905, São Carlos, SP, Brazil

ARTICLE INFO

Keywords:
Cr-doped glass
Lead silicate
Raman spectroscopy
XANES
UV–Vis

ABSTRACT

In this article the doping of chromium in a lead metasilicate glass is explored using Raman, UV–Vis, and Cr *K*-edge XANES spectroscopy. Our results indicate that the Cr ions are predominantly present as CrO_4^{2-} complexes, with a minor amounts of Cr(III). The solubility of Cr is limited to ~1 mol % Cr_2O_3. This boundary was inferred from the intensity changes to the CrO_4^{2-} stretching vibrations and confirmed by the inability to produce a homogeneous glass containing 2 mol % Cr_2O_3. The establishment of the solubility limit of Cr in lead glasses is important to design more effective glass compositions depending on the desired application. Finally, this low solubility indicates that Cr_2O_3 could be used as a potential nucleating agent for lead-silica based glass-ceramics.

1. Introduction

Chromium (Cr) doped glasses find a wide range of applications, e.g., in packaging [1], solid state lasers [2], as potential hosts for nuclear waste glasses [3], or even to improve protection from gamma rays [4–6]. All of these applications are dependent on how the Cr ions behave within the glass host, i.e., its oxidation state, local coordination, and concentration. In silicate glasses, Cr has been studied in all of its major forms from Cr(II) to Cr(VI) with oxygen coordination numbers from four to six [7,8]. The most common oxidation states are Cr(III) and Cr(VI). The former is generally found in low basicity glasses and/or under reducing atmosphere in octahedral geometry or as the phase eskolaite (Cr_2O_3) [9], while the latter is found under oxidizing conditions as mono- and/or dichromate complexes, CrO_4^{-2} and $Cr_2O_7^{-2}$ [7]. Examining the oxidation state, local geometry and solubility of Cr have motivated many investigations [3,10–12], as well as here, where we investigate Cr-doped lead metasilicate glass ($PbO{\cdot}SiO_2$; here called PS).

Due to its high stability, PS glass has been extensively investigated. [13–18], its structure [13], thermal [14,19,20] and optical [21] properties are well constrained. Based on our recent study [13], the tetrahedral network in PS is composed of 7% of Q^0, 25% Q^1, 38% of Q^2, 25% Q^3 and 5% Q^4, where Q^n represents a silicon tetrahedron with *n* bridging oxygens (Si–O–Si). Lead ions are present as PbO_4 polyhedral, with some PbO_5. This Q^n distribution is temperature dependent [13] and influences crystallization [19]. The optical properties of PS have been characterized by Dimitrov [21], who found a value of 1.859 for the refractive index and 2.92 eV for the optical bandgap. Optical absorption has also been used to investigate the effect of Cr addition in lead silicate glasses. Stroud [22] investigated the coloring effect of Cr on sodium-lead-silicate glasses. They concluded that Cr ions are present as Cr(VI), characterized by an absorption peak at 374 nm and a long wavelength tail that causes its yellow color. Baiocchi et al. [23] studied the addition of Cr to lead silicate glass with 37.9 mol % PbO, 0.3 mol % Pb_2O and 61.8 mol % SiO_2. Based on the optical absorption spectra, they associated the absorption cut off at 515.46 nm with the presence of Cr (VI) in tetrahedral sites, and the bands at 697, 658 and 630 nm with the presence of Cr(III) in octahedral sites. Additionally, Azooz and El Batal [4] explored the potential improvement in gamma shielding properties of the transition metals in a lead rich glass containing 71.24 mol % of PbO, 28.76 mol % of SiO_2. Using optical absorption, they found that Cr

* Corresponding author. Universidade Federal de Alagoas, Instituto de Física, 57072-900, Maceió, AL, Brazil.
E-mail addresses: dvsampaio@fis.ufal.br, davidvsampaio@gmail.com (D.V. Sampaio).

https://doi.org/10.1016/j.ceramint.2021.08.377
Received 13 June 2021; Received in revised form 19 August 2021; Accepted 30 August 2021
Available online 9 September 2021

addition retard the effect of gamma irradiation through the conversion of some Cr(VI) to Cr(III) capturing some liberated electrons in the irradiation processes. Aside from these investigations which focus on optical absorption, the evaluation of Cr doping in PS glass has not been explored in detail, as done below.

In this manuscript we investigate the solubility, oxidation state and local environment of Cr in a $PbO{\cdot}SiO_2$ (PS) glass. To tackle this problem, we use Raman spectroscopy, UV–Vis absorption and X-ray absorption near edge structure (XANES) spectroscopy at the Cr *K*-edge.

2. Experimental methods

Ten-gram batches of glasses were synthesized using PbO (Sigma Aldrich, 99.9%), SiO_2 (Vitrovita, Brazil) and CrO_3 (Sigma Aldrich, 99.9%). It is worth mentioning that a test comparing two Cr precursors reagents, Cr_2O_3 and CrO_3 (Sigma Aldrich, 99.9%), was done and evaluated using XANES (Sec. 3.3), and no distinction was detected in the final product. The precursor reagents were mixed using a high energy vibrating mill for 1 h to ensure a fine grained and homogenous powder was formed. Afterwards, the powder was melted at 900 °C for 20 min in an alumina crucible and then quenched by immersing the crucible in deionized water. The crucible was then broken and the glass chips were collected. The chemical compositions have been measured by electron probe microanalyzer (EPMA) on a JEOL JXA8230 5-WDS using a 15 nA current and 15 kV voltage on a 1 μm spot size. Table 1 shows the chemical analyses of the four glasses and the nomenclature used in this manuscript. Additional glasses were made with higher Cr concentrations, however, they **crystallized**.

Raman measurements were taken using Horiba-Jobin-Yvon HR800 Evolution micro-Raman spectrometer. A 488 nm wavelength laser was used as the excitation source and the scattered light was collected using a 50x super long work distance objective. The spectra were collected at ambient conditions using a 600 slits/mm grating between 10 and 1300 cm^{-1} with a laser power of 1 mW on the sample. The position of the silicon peak (520.7 cm^{-1}) was used to calibrate the spectrometer. For each sample a minimum of 5 spots were measured in order to check the sample homogeneity. The Raman spectra shown are area normalized after the background has been removed using a spline interpolation in Fityk software [24]. The same anchor points were used for background corrections. UV–Vis absorption measurements were performed using an Agilent UV-VIS-NIR Cary 5000 spectrophotometer in transmission mode. The samples were powdered and a fine layer was deposited on top of a slide for all measurements. The spectra were recorded at ambient conditions between 300 and 800 nm and are shown normalized to the maximum absorption.

The Cr *K*-edge (5989 eV) XANES spectra were collected on the XAFSII beamline at the Brazilian Synchrotron National Lab (LNLS) that operates with a 1.37 GeV electron storage ring and a maximum storage current of 250 mA [25,26]. The excitation energy was selected by a water-cooled Si(111) double crystal monochromator calibrated using a Cr metal foil by setting the inflection point to 5989.0 eV. All measurements were taken in fluorescence mode using a 15 Ge element detector, except the Cr_2O_3 standard that was measured in transmission mode. The measurement ranges were 5850–5987, 5987–6050 and 6050–6200 eV with energy steps of 3.0, 0.5 and 2 eV using a dwell time of 1, 5 and 2 s, respectively. The XANES measurements were taken on powdered samples that were pressed into 13 mm pellets containing a mixture of 14 mg of glass and 100 mg of boron nitride. A minimum of three scans were recorded for each sample and then averaged to produce the representative spectra presented below. The XANES spectrum of PS.06 (0.6 mol % Cr_2O_3) is not shown because of the low signal-to-noise at such a low Cr concentration. The normalization of all XANES spectra was performed using ATHENA [27], where the edge-step normalization was done using a linear fit to the pre-edge and a quadratic polynomial fit to the post-edge regions.

Table 1
Normalized chemical analysis of the glass samples reported in mol %.

Nomeclature	SiO_2	PbO	Al_2O_3	Cr_2O_3
PS	48.2	51.7	0.07	0
PS.06	47.7	52.4	0.02	0.06
PS.3	48.3	51.4	0.01	0.30
PS1	48.8	50.1	0.04	1.05

3. Results and discussion

3.1. Raman spectroscopy

Raman spectroscopy is an effective tool for investigating the structure of glass materials [28] [–] [30]. The PS-based glass has been recently studied in detail by Raman spectroscopy elsewhere [13,18,31]. Thus, it suffices to point out that the end-member PS glass has a Raman spectrum with all of the characteristic features expected [18] (Fig. 1): the boson peak around 40 cm^{-1}; two other bands at 100 cm^{-1} and 132 cm^{-1} associated with Pb ions; the intermediate frequencies show a small peak at 767 cm^{-1}, that has been attributed to Si–O vibrations; and, the asymmetric high frequency band related to the Q^n species. Comparing the spectrum of undoped PS to the Cr-doped samples indicates that new bands appear centered near 346, 376 and 830 cm^{-1} (Fig. 1). These additional bands have features that resemble the characteristic vibrational modes in crystalline $PbCrO_4$ (lead chromate, Fig. 2). Correlations between vibrational bands of Cr-doped glasses and chromate compounds have been pointed in some Cr(VI)-doped glasses [32,33] where the additional bands have been attributed to the formation of chromate (CrO_4^{2-}) molecules within the glass network [32–34]. Based on several Raman studies of crystalline $PbCrO_4$ [35–37], the low frequency bands (300–400 cm^{-1}) are attributed to the bending vibrations (deformation modes) of CrO_4^{2-} units. The additional high frequency modes (800–900 cm^{-1}) are due to symmetric stretching motions of these same units [34,38]. Therefore, we interpret the presence of the additional Raman bands at 346, 376 and 830 cm^{-1} in the Cr-doped PS glasses as originating from CrO_4^{2-} (chromate) complexes formed within these glasses, similarly to the chromate tetrahedra in the in $PbCrO_4$ (Fig. 3).

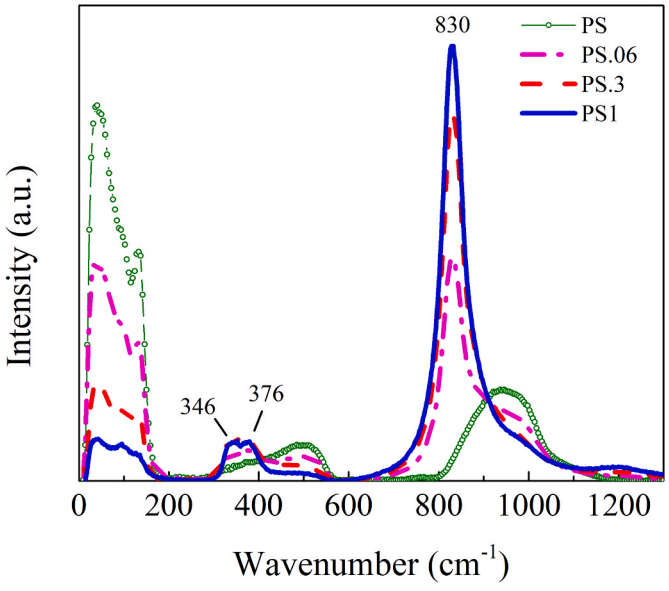

Fig. 1. Raman spectra of the pure PS and Cr-doped PS glasses as well as a $PbCrO_4$ standard. The addition of Cr in PS introduced new vibrational modes consistent with the modes found in $PbCrO_4$. These modes are identified as deformation modes (300–500 cm-1) and stretching motions (800–900 cm-1) of tetrahedral CrO_4^{2-} units.

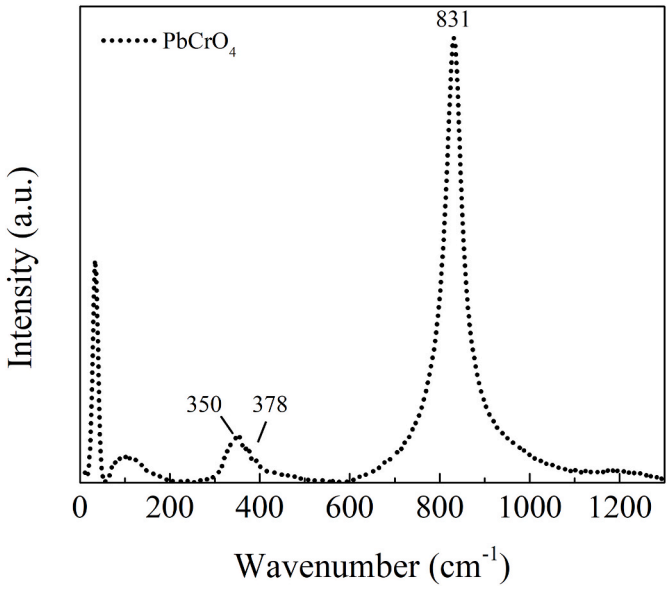

Fig. 2. Raman spectrum of $PbCrO_4$ emphasizing the peaks present in the Cr-doped glasses.

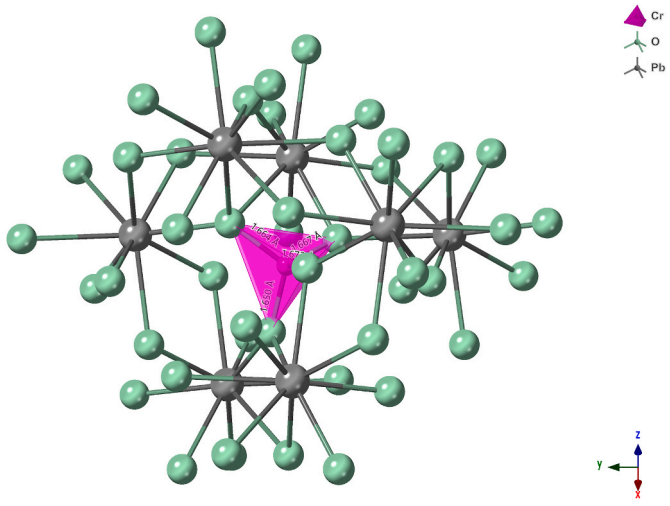

Fig. 3. Local structure of CrO_4^{2-} in $PbCrO_4$ [39], which is suggested to be similar to the local environment of Cr in PS glasses.

The superposition between the 830 cm^{-1} chromate Raman mode with the Q^n Raman band (800–1300 cm^{-1}) of the glass network precludes any estimation of the changes in the Q^n distribution network modification, using the Sampaio et al. curve fit model [13]. However, as discussed further below, the amount of Cr_2O_3 accepted by the network is as low as 1 mol %. At such low concentrations, we believe the presence of Cr will not have a major impact in the intermediate range order of the network. Therefore, we suggest that the effect of Cr_2O_3 addition on the glass structure is only a local structural effect from the formation of chromate complexes.

Notice in the spectra in Fig. 1 that, as the Cr concentration increases there is a dramatic increase in the intensity of the chromate-related modes. Thus, the intensity increases with increasing concentration of CrO_4^{2-} in the glass. In fact, the 830 cm^{-1} mode follows an exponential intensity increase (Fig. 4). The plateau in this exponential curve suggests that there is no further intensity increase after the sample has been doped with ~1 mol % Cr_2O_3 (e.g., at the PS1 composition). Therefore, we interpret this plateau as the solubility limit of Cr(VI) in PS glass.

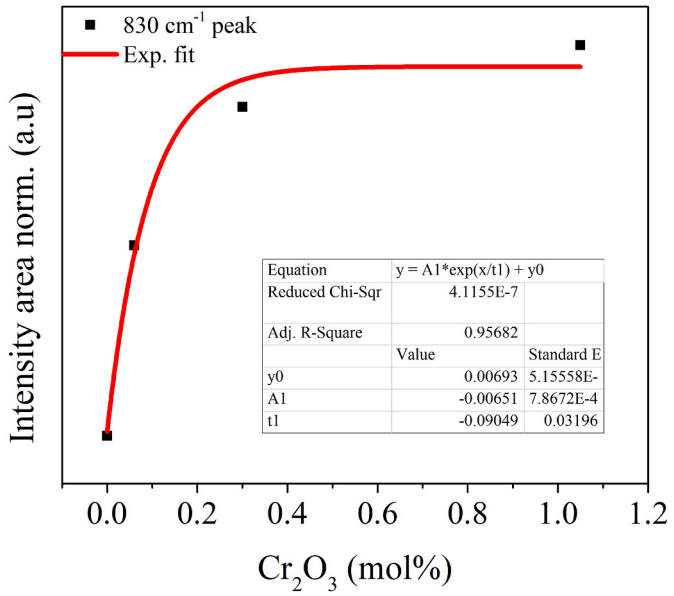

Fig. 4. Intensity of the band 830 cm^{-1} as a function of Cr_2O_3 concentration. At PS1 a plateau is observed, suggesting that the solubility limit has been reached. Higher concentrations led to crystallization of Cr_2O_3 which was detected by Raman spectroscopy (Fig. 5).

Hence, we propose that the chromate stretching vibrations (830 cm^{-1}) may indicate the solubility limit of Cr(VI) in the PS glass, and possibly in any lead-based glass, as lead ions seem to play an important role in the Cr incorporation mechanism into the lead silicate network through the formation of chromate complexes similarly to those found in $PbCrO_4$.

In order to check the solubility limit, we attempted to double the Cr concentration of PS1, producing a PS2 sample, with 2 mol % of Cr_2O_3. Raman spectra of this sample show that it is not a homogeneous glass. It is composed of regions of Cr-doped PS glass and regions of crystalline Cr_2O_3 (Fig. 5), corroborating our interpretation that the amount of Cr (VI) accepted into the PS glass matrix is limited to ~1 mol % Cr_2O_3 (or

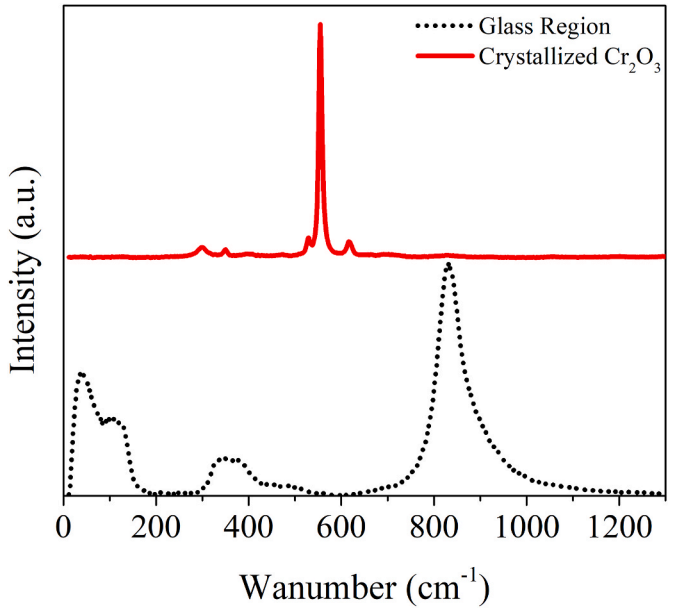

Fig. 5. The attempt to increase Cr concentration resulted in a non-homogeneous sample containing two chemically distinct regions. A glassy region, characterized by a typical Cr-doped PS glass spectrum, and a crystalline region, characterized by the Cr_2O_3 spectrum.

0.8 at. % of Cr). This solubility limit is low compared to soda silicate glasses but is in the range of soda-lime silicate glasses [40,41]. This low solubility also suggests that Cr_2O_3 may be a useful nucleating agent for lead-silica based glass-ceramics. However, these would be yellow-reddish colored.

The literature shows that Cr solubility in soda silicate (Na_2O-$xSiO_2$) and soda-lime silicate (Na_2O–CaO-$xSiO_2$) glasses depends on the melting temperature, oxygen fugacity (fO_2) and composition [40,41]. Under an oxidizing atmosphere (e.g., air), the Cr solubility increases from ~1 to ~3 at. % as x decreases from 3.5 to 1.5 in the Na_2O-$xSiO_2$ system [40]. A similar behavior is observed in Na_2O–CaO-$xSiO_2$, where the Cr solubility limit increases from ~0.4 to ~1 at. % as x decreases from 7 to 3 [41]. Based on these studies [40,41], we suggest that the addition of lead into the silicate network may increase the solubility limit of Cr_2O_3. This objective is currently being tested and will be the focus of a future work.

3.2. Optical absorption

The Cr-doped PS glasses display a yellow-reddish coloration in contrast to pure PS glass which is colorless. The glasses become more reddish as the Cr_2O_3 concentration increases from 0.03 to 1.0 mol %. This color change is reflected in the absorption measurement by an edge shift and the appearance of several weak bands between 550 and 750 nm (Fig. 6). The pure PS glass shows a strong absorption below ~380 nm due to Pb^{2+} and matrix transitions [11]. Above this wavelength, the glass is essentially transparent. Cr addition, even at very low Cr concentrations (e.g., 0.06 mol %), drastically changes the spectrum which shows a strong absorption below ~500 nm and additional weak bands between 550 and 750 nm (inset Fig. 6). These weak absorption bands are attributed to the presence of Cr(III) in an octahedral site [10,23], and are identified as the $^4A_2 \rightarrow {}^4T_2$ spin allowed, $^4A_2 \rightarrow {}^2E$ and $^4A_2 \rightarrow {}^2T_1$ spin-forbidden transitions.

The wavelength dependence of the strong absorption can be quantified by the estimative of the optical absorption edge, the maximum of the first derivative of the absorption spectra [18] (Fig. 7). Note that the inset in Fig. 7 shows that the absorption edge decreases from 3.4 to 2.4 eV as Cr concentration increases. According to Stroud [22] and Baiochi et al. [23], the change in the absorption edge can be attributed to Cr(VI), present as chromate groups, CrO_4^{2-}. Therefore, the continuous decrease in the absorption edge suggests an increase in the amount of chromate groups, corroborating the Raman analysis above.

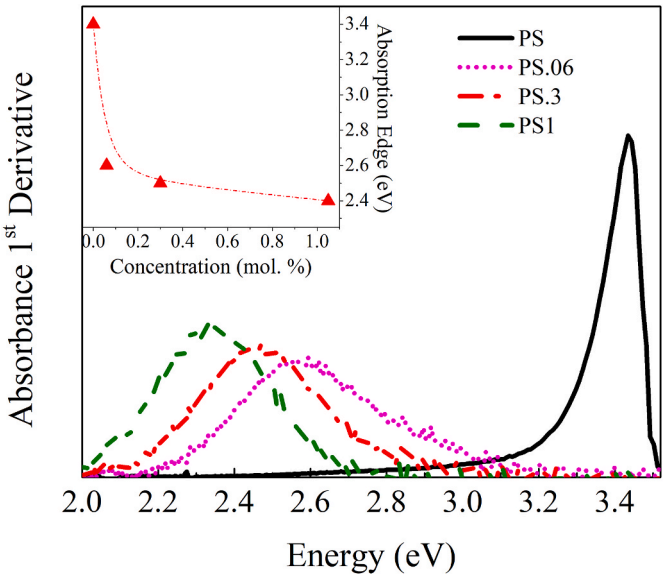

Fig. 7. Change of gap energy with Cr_2O_3 concentration. The first derivative maximum is used to estimate the band gap energy change.

3.3. X-ray absorption spectroscopy

The Cr K-edge XANES spectra are sensitive to both the valence state and the local environment. Fig. 8 shows the Cr K-edge XANES spectra of three Cr doped glasses, two of them with the same Cr content (1 mol %) that were produced using two different precursor reagents, Cr_2O_3 (PS1–Cr_2O_3) and CrO_3 (PS1–CrO_3), and the other having a lower Cr content (PS.3, 0.3 mol %). Note that all of them resulted in glasses with the same Cr K-edge spectrum. Therefore, neither the use of distinct Cr reagents nor the concentration affects the Cr oxidation state or environment within these PS glasses. In addition, comparing the spectra of the Cr-doped glasses to the oxide standards (Fig. 9) shows that there is a clear the similarity between the glass spectra and that of $PbCrO_4$ [42].

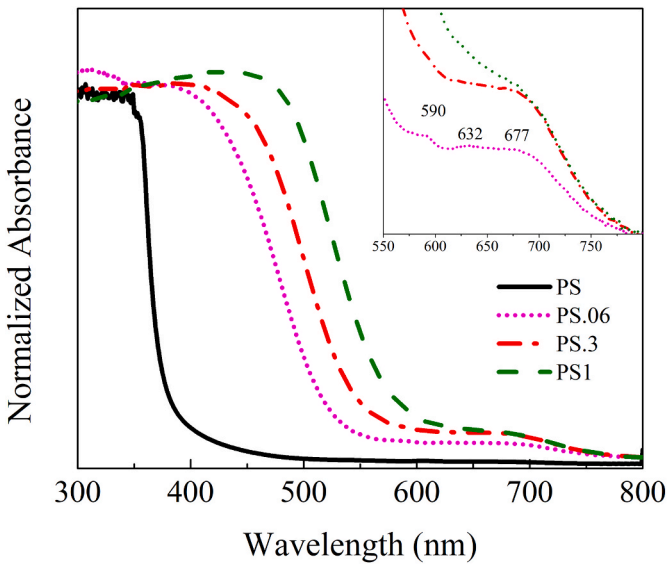

Fig. 6. UV–Vis absorption spectrum showing a red shift with the introduction of Cr. This red shift is related to the increase of chromate groups. (For interpretation of the references to color in this figure legend, the reader is referred to the Web version of this article.)

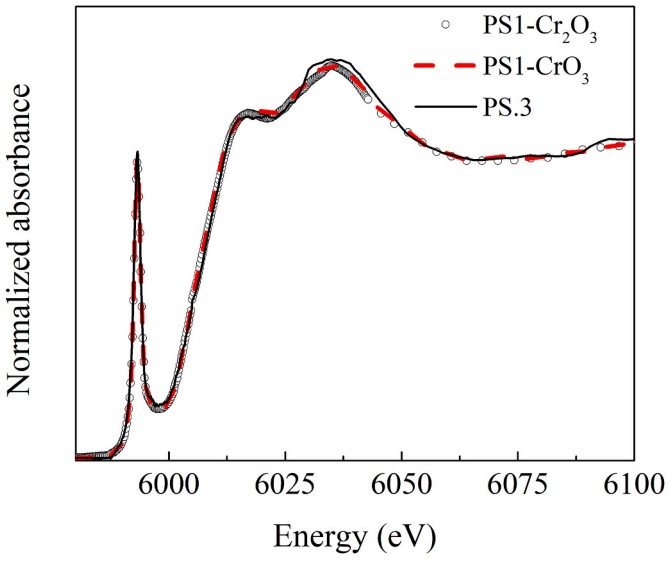

Fig. 8. Cr K-edge spectra of Cr-doped PS glasses synthesized with different Cr precursor reagents (either Cr_2O_3 or CrO_3) and different concentrations. These spectra show that neither the precursor source nor the Cr concentration influence the final glass producing in terms of the oxidation state or local environment of Cr.

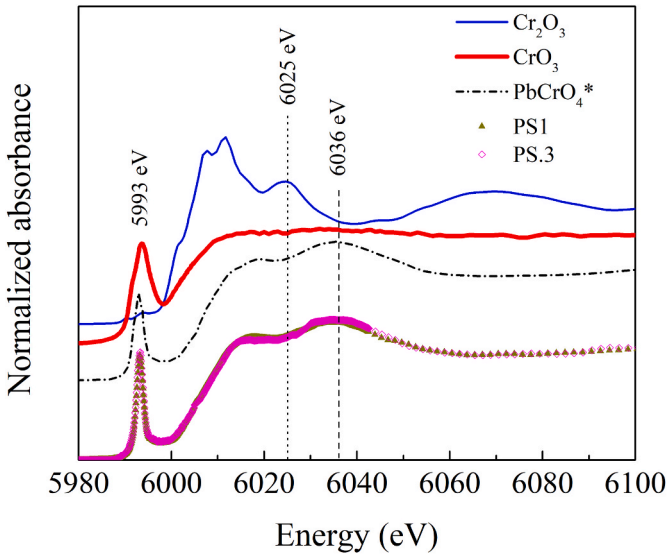

Fig. 9. Cr *K*-edge spectra of Cr-containing glasses and standards. According to these spectra, the Cr(VI)/Cr(III) ratio does not depend on the Cr content and the glasses show similar features as found in crystalline $PbCrO_4$, confirming that Cr (VI) is present in the glasses in a similar environment to that in $PbCrO_4$. *Data extracted from Ref. [42].

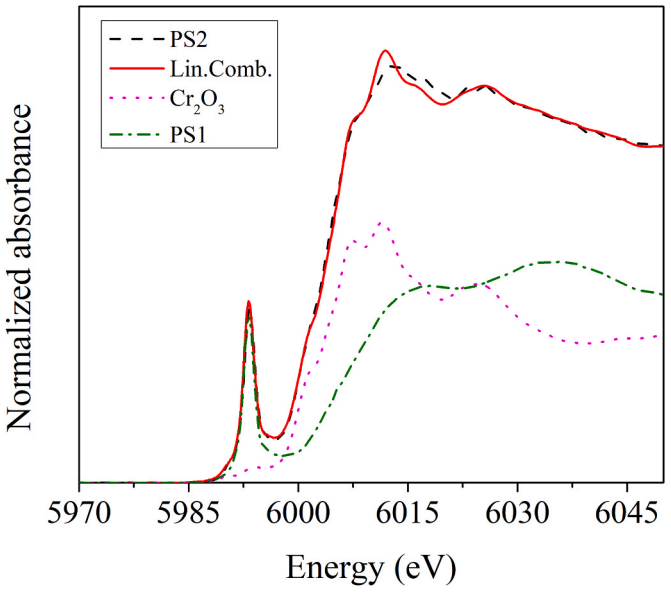

Fig. 10. Estimation of the Cr_2O_3 segregation using a linear combination fitting of Cr_2O_3 and PS1 glass spectra. This combination indicates that 53% of the signal of the total Cr content can be attributed to crystalline Cr_2O_3 and 47% is present as Cr(VI) in the glass matrix.

This reinforces our interpretation of the Raman spectra above that the chemical environment of Cr in PS glass is similar to that found in $PbCrO_4$.

The spectra of the PS1 and PS.3 glasses (Fig. 8) show a very pronounced pre-edge peak at 5993 eV, that is also observed in the CrO_3 and $PbCrO_4$ spectra (Fig. 9). It is well known that this peak is related to the electronic transitions between the 1s and 3d orbitals occurring predominantly for Cr(VI) in a non-centrosymmetric tetrahedral geometry [43–45]. It is also established that this pre-edge peak is proportional to the Cr(VI)/Cr(III) ratio. Peterson et al. [44] have shown that it is possible to quantify the proportion of Cr(VI) in a sample if its fraction is > 1–5% of the total Cr. Here, the pre-edge peak of the glass has the same intensity as that of the CrO_3 standard. This would lead us to infer that the content of Cr(VI) in the glasses is 100%. However, our UV–Vis absorption measurements have clearly shown the presence of Cr(III). Therefore, the Cr(VI) fraction present in PS1, PS.3 is close to, but not, 100%, where a more accurate quantification is limited by the measurement sensitivity.

As mentioned before, the attempt to increase the Cr concentration above 1 mol % resulted in the crystallization of Cr_2O_3 in PS2 glass matrix (Section 3.1). To estimate the amount of Cr_2O_3 segregated compared to the Cr(VI) dissolved into the PS2 glass host, we used a linear combination fitting of the standard Cr_2O_3 and PS1 spectra to reproduce the PS2 Cr *K*-edge spectrum (Fig. 10). This is commonly done to estimate Cr(VI)/Cr(III) ratio when standard references are available [1,42,46,47]. Following Kappen et al. [42], using the energy region between 5970 and 6050 eV in the fit, the signal of Cr_2O_3 is calculated to be 53%. Assuming that the signal is directly proportional to the concentration, and despite the aforementioned experimental limitation, it is estimated that 53% is segregated as Cr_2O_3 and the remaining 47% of Cr is homogeneously dispersed in the glass matrix, with a large majority as Cr(VI) in CrO_4^{2-}.

4. Summary and conclusions

We investigated the doping of Cr ions into lead metasilicate glasses by varying the Cr content and determining its oxidation state and local environment. Based on the Raman, UV–Vis absorption, and XANES measurements we conclude that Cr is predominantly found as $Cr_2O_4^{2-}$ complexes surrounded by Pb ions in a similar geometry as found in crystalline $PbCrO_4$. On the other hand, UV–vis absorption measurements show a small proportion of Cr(III) octahedra are also present.

The solubility limit of Cr_2O_3 in the glass host is around 1 mol %. This limit was inferred from the exponential growth behavior of the CrO_4 stretching mode (831 cm^{-1}) in Raman spectra and confirmed by the failed attempt to produce a homogeneous glass with 2 mol % chromium oxide. This attempt resulted in the precipitation of Cr_2O_3 crystals. Therefore, this oxide could be a potential nucleating agent for lead-silica-based glass-ceramics.

We estimate that about half of the total Cr content of the 2 mol % Cr-doped sample was present as Cr_2O_3 crystals and half as $Cr_2O_4^{2-}$ complexes diluted in the glass host, consistent with the determined solubility limit. These conclusions are essential to design Cr-doped lead silicate glasses and to explore new glass-ceramic systems.

Declaration of competing interest

The authors declare that they have no known competing financial interests or personal relationships that could have appeared to influence the work reported in this paper.

Acknowledgements

The authors are thankful to FAPESP for the CEPID project funding (no. 2013/07793-6). DVS, BJAM, RBP and TRC are also grateful to FAPESP for the research grants no. 2016/15962-0, 2016/18567-5, 2017/11868-2 and 2019/12383-8, respectively. We also thank CAPES and CNPq (409017/2016-7) Brazilian agencies for financial support. Finally, we would like to acknowledge the LNLS (proposal 20170129) and especially the XAFSII beamline staff, Santiago Figueroa, Junior Mauricio and Carlos Neto, for their excellent help.

References

[1] O. Villain, G. Calas, L. Gaioisy, L. Cormier, J.-L. Hazemann, XANES determination of chromium oxidation states in glasses: comparison with optical absorption spectroscopy, J. Am. Ceram. Soc. 90 (2007) 3578–3581, https://doi.org/10.1111/j.1551-2916.2007.01905.x.

[2] T. Murata, M. Torisaka, H. Takebe, K. Morinaga, Compositional dependence of the valency state of Cr ions in oxide glasses, J. Non-Cryst. Solids 220 (1997) 139–146, https://doi.org/10.1016/S0022-3093(97)00264-0.

[3] H. Zhu, Q. Liao, F. Wang, Y. Dai, M. Lu, The effects of chromium oxide on the structure and properties of iron borophosphate glasses, J. Non-Cryst. Solids 437 (2016) 48–52, https://doi.org/10.1016/j.jnoncrysol.2016.01.013.

[4] M.A. Azooz, F.H. ElBatal, Gamma ray interaction with transition metals-doped lead silicate glasses, Mater. Chem. Phys. 117 (2009) 59–65, https://doi.org/10.1016/j.matchemphys.2009.04.038.

[5] B. Aktas, S. Yalcin, K. Dogru, Z. Uzunoglu, D. Yilmaz, Structural and radiation shielding properties of chromium oxide doped borosilicate glass, Radiat. Phys. Chem. 156 (2019) 144–149, https://doi.org/10.1016/j.radphyschem.2018.11.012.

[6] A.I. Ismail, A. Samir, F. Ahmad, L.I. Soliman, A. Abdelghany, Spectroscopic studies and the effect of radiation of alkali borate glasses containing chromium ions, J. Non-Cryst. Solids 565 (2021) 120743, https://doi.org/10.1016/j.jnoncrysol.2021.120743.

[7] F. Farges, Chromium speciation in oxide-type compounds: application to minerals, gems, aqueous solutions and silicate glasses, Phys. Chem. Miner. 36 (2009) 463–481, https://doi.org/10.1007/s00269-009-0293-3.

[8] A.J. Berry, H.S.C. O'Neill, A XANES determination of the oxidation state of chromium in silicate glasses, Am. Mineral. 89 (2004) 790–798, https://doi.org/10.2138/am-2004-5-613.

[9] P. Hrma, J.D. Vienna, B.K. Wilson, T.J. Plaisted, S.M. Heald, Chromium phase behavior in a multi-component borosilicate glass melt, J. Non-Cryst. Solids 352 (2006) 2114–2122, https://doi.org/10.1016/j.jnoncrysol.2006.02.051.

[10] R. Lachheb, A. Herrmann, K. Damak, C. Rüssel, R. Maâlej, Optical absorption and photoluminescence properties of chromium in different host glasses, J. Lumin. 186 (2017) 152–157, https://doi.org/10.1016/j.jlumin.2017.02.030.

[11] H. Wen, P.A. Tanner, B.-M. Cheng, Optical properties of $3d^N$ transition metal ion-doped lead borate glasses, Mater. Res. Bull. 83 (2016) 400–407, https://doi.org/10.1016/j.materresbull.2016.06.032.

[12] O. Villain, L. Galoisy, G. Calas, Spectroscopic and structural properties of Cr^{3+} in silicate glasses: Cr^{3+} does not probe the average glass structure, J. Non-Cryst. Solids 356 (2010) 2228–2234, https://doi.org/10.1016/j.jnoncrysol.2010.08.028.

[13] D.V. Sampaio, A. Picinin, B.J.A. Moulton, J.P. Rino, P.S. Pizani, E.D. Zanotto, Raman scattering and molecular dynamics investigation of lead metasilicate glass and supercooled liquid structures, J. Non-Cryst. Solids 499 (2018) 300–308, https://doi.org/10.1016/j.jnoncrysol.2018.07.048.

[14] D.R. Cassar, R.F. Lancelotti, R. Nuernberg, M.L.F. Nascimento, A.M. Rodrigues, L. T. Diz, et al., Elemental and cooperative diffusion in a liquid, supercooled liquid and glass resolved, J. Chem. Phys. 147 (2017), 014501, https://doi.org/10.1063/1.4986507.

[15] S. Feller, G. Lodden, A. Riley, T. Edwards, J. Croskrey, A. Schue, et al., A multispectroscopic structural study of lead silicate glasses over an extended range of compositions, J. Non-Cryst. Solids 356 (2010) 304–313, https://doi.org/10.1016/j.jnoncrysol.2009.12.003.

[16] S. Kohara, H. Ohno, M. Takata, T. Usuki, H. Morita, K. Suzuya, et al., Lead silicate glasses: binary network-former glasses with large amounts of free volume, Phys. Rev. B 82 (2010) 134209, https://doi.org/10.1103/PhysRevB.82.134209.

[17] R.B. Pena, V. Laurent, T. Deschamps, E. Romeo, A. Picinin, C. Martinet, et al., High-pressure plastic deformation of lead metasilicate glass accessed by Raman spectroscopy: insights into the Qn distribution, J. Non-Cryst. Solids 567 (2021) 120930, https://doi.org/10.1016/j.jnoncrysol.2021.120930.

[18] D.C. Silva, D.V. Sampaio, J.H.L. Silva, A.M. Rodrigues, R.B. Pena, B.J.A. Moulton, et al., Synthesis of $PbO{\cdot}SiO_2$ glass by CO_2 laser melting method, J. Non-Cryst. Solids 522 (2019) 119572, https://doi.org/10.1016/j.jnoncrysol.2019.119572.

[19] R.B. Pena, D.V. Sampaio, R.F. Lancelotti, T.R. Cunha, E.D. Zanotto, P.S. Pizani, In-situ Raman spectroscopy unveils metastable crystallization in lead metasilicate glass, J. Non-Cryst. Solids 546 (2020) 120254, https://doi.org/10.1016/j.jnoncrysol.2020.120254.

[20] R.F. Lancelotti, D.R. Cassar, M. Nalin, O. Peitl, E.D. Zanotto, Is the structural relaxation of glasses controlled by equilibrium shear viscosity? J. Am. Ceram. Soc. 104 (2021) 2066–2076, https://doi.org/10.1111/jace.17622.

[21] V.V. Dimitrov, S.-N. Kim, T. Yoko, S. Sakka, Third harmonic generation in $PbO{-}SiO_2$ and $PbO{-}B_2O_3$ glasses, J. Ceram. Soc. Japan. 101 (1993) 59–63, https://doi.org/10.2109/jcersj.101.59.

[22] J.S. Stroud, Optical absorption and color caused by selected cations in high-density, lead silicate glass, J. Am. Ceram. Soc. 54 (1971) 401–406, https://doi.org/10.1111/j.1151-2916.1971.tb12331.x.

[23] E. Baiocchi, A. Montenero, M. Bettinelli, A. Sotgiu, Optical and magnetic properties of first-row transition metal ions in lead-silicate glass, J. Non-Cryst. Solids 46 (1981) 203–215, https://doi.org/10.1016/0022-3093(81)90161-7.

[24] M. Wojdyr, *Fityk* : a general-purpose peak fitting program, J. Appl. Crystallogr. 43 (2010) 1126–1128, https://doi.org/10.1107/S0021889810030499.

[25] H.C. Tolentino, A.Y. Ramos, M.C. Alves, R.A. Barrea, E. Tamura, J.C. Cezar, et al., A 2.3 to 25 keV XAS beamline at LNLS, J. Synchrotron Radiat. 8 (2001) 1040–1046, https://doi.org/10.1107/s0909049501005143.

[26] S.J.A. Figueroa, J.C. Mauricio, J. Murari, D.B. Beniz, J.R. Piton, H.H. Slepicka, et al., Upgrades to the XAFS2 beamline control system and to the endstation at the LNLS, J. Phys.: Conf. Ser. 712 (2016), 012022, https://doi.org/10.1088/1742-6596/712/1/012022.

[27] B. Ravel, M. Newville, ATHENA, artemis, hephaestus: data analysis for X-ray absorption spectroscopy using IFEFFIT, J. Synchrotron Radiat. 12 (2005) 537–541, https://doi.org/10.1107/S0909049505012719.

[28] S. Rossano, B. Mysen, Raman spectroscopy of silicate glasses and melts in geological systems, in: G. Ferraris, J. Dubessy, M.C. Caumon, F. Rull (Eds.), Raman Spectroscopy Applied to Earth Sciences and Cultural Heritage, European Mineralogical Union, 2012, pp. 321–366, https://doi.org/10.1180/EMU-notes.12.9.

[29] B.J.A. Moulton, A.M. Rodrigues, P.S. Pizani, D.V. Sampaio, E.D. Zanotto, A Raman investigation of the structural evolution of supercooled liquid barium disilicate during crystallization, Int. J. Appl. Glass Sci. 9 (2018) 510–517.

[30] G.S. Henderson, L.G. Soltay, H.M. Wang, Q speciation in alkali germanate glasses, J. Non-Cryst. Solids 356 (2010) 2480–2485, https://doi.org/10.1016/j.jnoncrysol.2010.03.023.

[31] I. Ben Kacem, L. Gautron, D. Coillot, D.R. Neuville, Structure and properties of lead silicate glasses and melts, Chem. Geol. 461 (2017) 104–114, https://doi.org/10.1016/j.chemgeo.2017.03.030.

[32] S.A. Brawer, W.B. White, Raman spectroscopic study of hexavalent chromium in some silicate and borate glasses, Mater. Res. Bull. 12 (1977) 281–287, https://doi.org/10.1016/0025-5408(77)90146-5.

[33] C. Nelson, T. Furukawa, W.B. White, Transition metal ions in glasses: network modifiers or quasi-molecular complexes? Mater. Res. Bull. 18 (1983) 959–966, https://doi.org/10.1016/0025-5408(83)90007-7.

[34] E.C. Ziemath, M.A. Aegerter, F.E.A. Melo, J.E. Moreira, J. Mendes Filho, M.S. S. Dantas, et al., Pre-resonant Raman effect of CrO_4^{2-} in a metasilicate glass, J. Non-Cryst. Solids 194 (1996) 41–47, https://doi.org/10.1016/0022-3093(95)00492-0.

[35] E. Bandiello, D. Errandonea, D. Martinez-Garcia, D. Santamaria-Perez, F.J. Manjón, Effects of high-pressure on the structural, vibrational, and electronic properties of monazite-type PbCrO, Phys. Rev. B 85 (2012), 024108, https://doi.org/10.1103/PhysRevB.85.024108.

[36] R.W.T. Wilkins, The Raman spectrum of crocoite, Mineral. Mag. 38 (1971) 249–250, https://doi.org/10.1180/minmag.1971.038.294.15.

[37] W. Scheuermann, G.J. Ritter, The vibrational spectra of strontium chromate ($SrCrO_4$) and lead chromate ($PbCrO_4$), zeitschrift fur naturforschung a 25 (1970) 1856–1862, https://doi.org/10.1515/zna-1970-1212.

[38] L. Monico, K. Janssens, E. Hendriks, B.G. Brunetti, C. Miliani, Raman study of different crystalline forms of $PbCrO_4$ and $PbCr_{1-x}S_xO_4$ solid solutions for the noninvasive identification of chrome yellows in paintings: a focus on works by Vincent van Gogh, J. Raman Spectrosc. 45 (2014) 1034–1045, https://doi.org/10.1002/jrs.4548.

[39] H. Effenberger, F. Pertlik, Four monazite type structures: comparison of $SrCrO_4$, $SrSeO_4$, $PbCrO_4$(crocoite), and $PbSeO_4$, Z. für Kristallogr. - Cryst. Mater. 176 (1986), https://doi.org/10.1524/zkri.1986.176.12.75.

[40] H. Khedim, R. Podor, C. Rapin, M. Vilasi, Redox-Control solubility of chromium oxide in soda-silicate melts, J. Am. Ceram. Soc. 91 (2008) 3571–3579, https://doi.org/10.1111/j.1551-2916.2008.02692.x.

[41] H. Khedim, T. Katrina, R. Podor, P.-J. Panteix, C. Rapin, M. Vilasi, Solubility of Cr_2O_3 and speciation of chromium in soda-lime-silicate melts, J. Am. Ceram. Soc. (2010), https://doi.org/10.1111/j.1551-2916.2009.03581.x.

[42] P. Kappen, E. Welter, P.H. Beck, J.M. McNamara, K.A. Moroney, G.M. Roe, et al., Time-resolved XANES speciation studies of chromium on soils during simulated contamination, Talanta 75 (2008) 1284–1292, https://doi.org/10.1016/j.talanta.2008.01.041.

[43] Y.G. Choi, K.H. Kim, Y.S. Han, J. Heo, Oxidation state and local coordination of chromium dopant in soda-lime-silicate and calcium-aluminate glasses, Chem. Phys. Lett. 329 (2000) 370–376, https://doi.org/10.1016/S0009-2614(00)01054-X.

[44] M.L. Peterson, G.E. Brown, G.A. Parks, Quantitative determination of chromium valence in environmental samples using xafs spectroscopy, MRS Proc 432 (1996) 75, https://doi.org/10.1557/PROC-432-75.

[45] M.L. Peterson, G.E. Brown, G.A. Parks, C.L. Stein, Differential redox and sorption of Cr (III/VI) on natural silicate and oxide minerals: EXAFS and XANES results, Geochem. Cosmochim. Acta 61 (1997) 3399–3412, https://doi.org/10.1016/S0016-7037(97)00165-8.

[46] L. Monico, G. Van der Snickt, K. Janssens, W. De Nolf, C. Miliani, J. Verbeeck, et al., Degradation process of lead chromate in paintings by Vincent van Gogh studied by means of synchrotron X-ray spectromicroscopy and related methods. 1. Artificially aged model samples, Anal. Chem. 83 (2011) 1214–1223, https://doi.org/10.1021/ac102424h.

[47] L. Monico, K. Janssens, E. Hendriks, F. Vanmeert, G. Van der Snickt, M. Cotte, et al., Evidence for degradation of the chrome yellows in van gogh's sunflowers: a study using noninvasive in situ methods and synchrotron-radiation-based X-ray techniques, Angew Chem. Int. Ed. Engl. 54 (2015) 13923–13927, https://doi.org/10.1002/anie.201505840.